


Numerical and experimental stress analysis of an internal-combustion engine valve during the closing event

Proc IMechE Part D:
J Automobile Engineering
2014, Vol. 228(5) 479–489
© IMechE 2014
Reprints and permissions:
sagepub.co.uk/journalsPermissions.nav
DOI: 10.1177/0954407013498862
pid.sagepub.com


Federico J Cavalieri¹, César Luengo¹, José Risso¹, Fernando Zenklusen²
and Alberto Cardona¹

Abstract

This paper presents a numerical methodology to predict the stress evolution in an internal-combustion engine valve during the closing event. The problem is studied using a three-dimensional finite element model, showing that the seating process of the valve produces high bending stresses which are not demonstrated by two-dimensional models. The valve stem stress response under impact was registered experimentally using strain gauges and then compared with the finite element method solutions, showing good agreement. The main contribution of this paper is the identification of the factors which generate the development of impact stresses during the closing event in an internal-combustion engine valve and which could result in fatigue failure.

Keywords

Engine modelling, valvetrain system, structural integrity, impact dynamics, valve closing event

Date received: 6 November 2012; accepted: 19 June 2013

Introduction

To satisfy market demands, engine manufacturers are required to increase the strength of their engines and to extend the time required between servicing checks. New materials and production methodologies are being introduced to obtain cost-effective techniques to be applied to the new developments.

The two main types of automotive internal-combustion engine are based on the Otto cycle and the Diesel cycle, where poppet valves control the intake gas flow and the exhaust gas flow in the cylinders. During the intake stroke, the intake valve is opened; in the compression stroke, both the intake valve and the exhaust valve are closed; the exhaust valve opens during the expansion stroke; finally, the exhaust valve remains open in the exhaust stroke. The valves work under very stringent conditions with very low lubrication, imposed by environmental considerations, and should last for an operative lifetime of up to 10^8 cycles or more; therefore, it is necessary to investigate the fatigue behaviour of valve materials^{1–3} produced by the repetitive stress peaks during the closing event in the engine, in order to improve designs.^{4,5} A good understanding of the different mechanisms that govern the development of stresses over time in the component is

required. Numerical methods are a valuable tool for this assessment. Rahnejat⁶ gave a general overview of the different numerical and experimental techniques used in engine dynamics.

During the closing event of an engine valve, high impact stresses are developed when the valve hits the seat insert at the end of each closing motion. The magnitude of these stresses depends on various factors such as, first, the return spring stiffness, second, the inertia loads of the retainer, the keeper and the stem, third, the closing velocity and, fourth, the valve tilt and the thermal loads induced by the combustion. The mechanical stresses developed on the valve stem during this event are considered to be one of the most significant factors in the design of valves. Stem stresses are variable in time

¹Centro Internacional de Métodos Computacionales en Ingeniería, Universidad Nacional del Litoral, Consejo Nacional de Investigaciones Científicas y Técnicas, Santa Fe, Argentina

²MAHLE Argentina SA, Santa Fe, Argentina

Corresponding author:

Federico J Cavalieri, Centro Internacional de Métodos Computacionales en Ingeniería, Universidad Nacional del Litoral, Consejo Nacional de Investigaciones Científicas y Técnicas, Güemes 3450, S3000GLN, Santa Fe, Argentina.

Email: fcavalieri@santafe-conicet.gov.ar

and propagate mainly as stress waves in the axial direction along the valve stem. Therefore, an understanding of the closing event and knowledge of the values of the maximum stresses are necessary to design a new valve for a specific operative lifetime.

Several multi-body models have been proposed to evaluate the stresses in valvetrain components. Some of these are lumped-mass models, consisting of constrained multi-body dynamic systems with sources of compliance in the valvetrain. In these models, the motion characteristics and the dynamic properties are simplified, neglecting the impulsive non-linear forces. For instance, in the work of Teodorescu et al.,⁵ a multi-body one-dimensional (1D) dynamic model was used to predict the vibration and forces in a valvetrain system. As mentioned by these researchers, this model is not able to obtain the impact stresses, and a separated impact model is needed. Experimental strain measurements in the valves indicate that the developed stress pattern at the closing instant is not 1D because three-dimensional (3D) effects develop on the stem cross-section, as reported by Roth.^{7,8} The closing event consists, in fact, of a sequence of phases motivated by the eccentricity arising from the assembly tolerances of the valvetrain components, as discussed in this work.

The use of numerical simulation tools for the prediction of stresses and strains, specifically the finite element method (FEM),^{9,10} can help in the design of valves when considering different materials, geometries and valvetrain configurations.¹¹ However, to validate the FEM as a design tool, appropriate parameters for the time integration algorithm have to be determined to obtain reliable solutions in a reasonable computational time. Some researchers have used multi-body lumped models coupled with finite element models¹² or analytical two-degree-of-freedom systems^{13,14} to simulate the valvetrain in a reduced computing time, although none of these models is capable of demonstrating 3D effects, such as the eccentric seating of the valve.

If the focus of the analysis is the assessment of the impact wear in the seating zone, hard wear-resistant coatings have to be considered in the model to predict properly the contact pressure distribution of the contacting bodies. The thickness of these layers can also be predicted by using the FEM as proposed by Votsios,¹⁵ Konvopoulos and Gong¹⁶ and Overat and Pan.¹⁷ However, these approaches are time consuming because very thin elements must be used for the coating mesh and because they result in a very large number of nodes, particularly in 3D cases. Another methodology able to predict the behaviour of the bonded coating bodies in a faster way than the FEM was proposed by Teodorescu and Rahnejat,¹⁸ although it is restricted to the two-dimensional case. Some extensions of this work could be implemented in general 3D cases to study, for example, the contact pressure during the closing event of the valve. However, as the main objective of this work is to study the stresses in the stem, the hard coatings of the valve and the seat were not taken into account in this research.

Often, automotive engine valve manufacturers design valves using classical engineering formulae, by considering the part as a simply supported circular flat plate with a uniformly distributed load¹⁹ or by using a linear FEM model under equivalent static load conditions. Although results are obtained in a relatively short time with these methodologies, they can lead to inefficient conservative designs that increase manufacturing costs. In this work, a 3D finite element model of a valve was constructed, with the aim of evaluating the dynamic effects at the impact between the valve and the seat insert. The numerical solutions were analysed and compared with the physical measurements obtained on an instrumented valve, which was assembled and operated in a cylinder head. The main objective of this study was to obtain a better understanding of the phenomena which occur during the valve closing event, through the numerical evaluation of the response and the analysis of experimental strain data measurements at room temperature. A precise description of the different phenomena developed during valve closure was obtained. Moreover, the following secondary objectives were pursued:

- (a) development of a numerical model for displacement and stress calculation at different points on the valve;
- (b) calibration of the numerical time integration algorithms to minimize the computational time while giving reliable solutions;
- (c) validation of the numerical solutions with the obtained experimental data to apply the numerical valve model in order to analyse new valve designs.

The work is organized as follows. The section on experimental stress measurements describes the experimental procedure and the strain measurements obtained in an instrumented valve. In the section on the definition of the numerical model, a numerical model of a valve is presented, including the physical and numerical parameters together with the numerical stress solutions. Then, a comparison between the experimental results and the numerical solutions is presented in the section on the analysis of results; conclusions are given in the final section.

Experimental stress measurements

The tests were conducted using a specially designed engine valvetrain test bench, which was developed in co-operation with Oreste Berta SA.²⁰

The first stage of this work was to make experimental strain measurements on an instrumented valve. Tests were conducted at room temperature in an exhaust valve of a naturally aspirated 1.6 l Otto engine with four cylinders and two valves per cylinder, a power of 74 kW at 5500 r/min and a torque of 153 Nm at 2500 r/min.

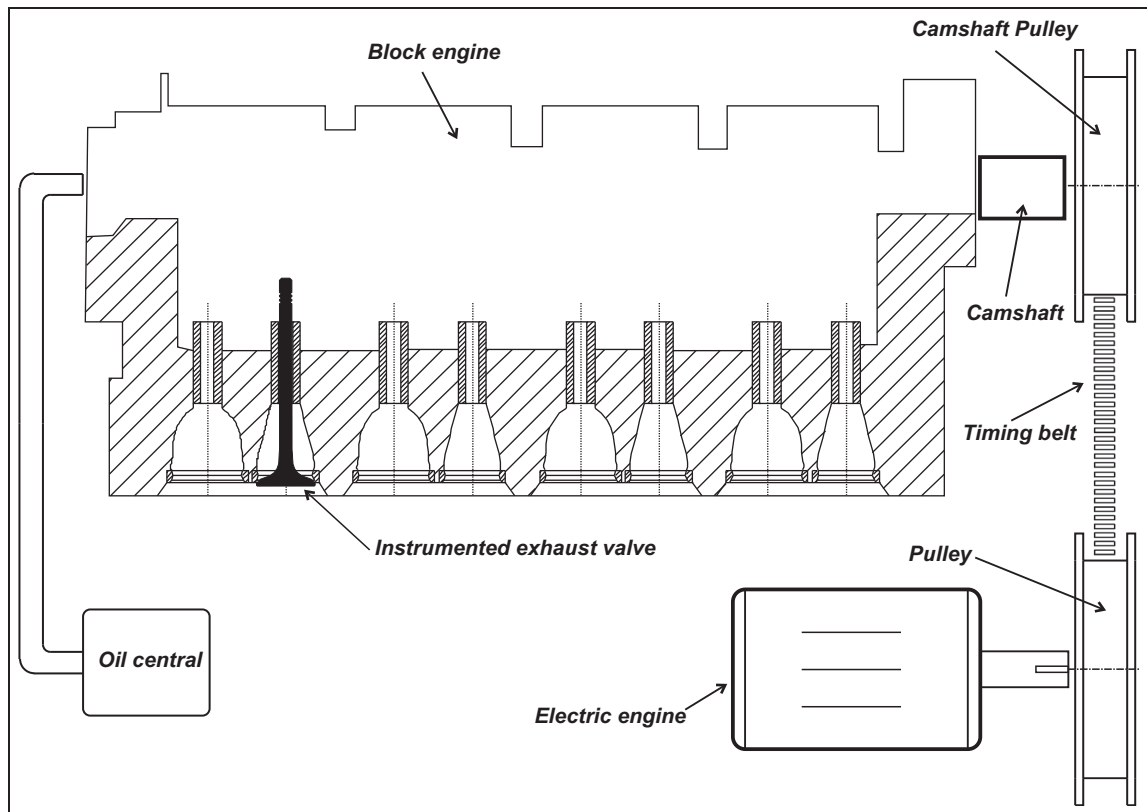


Figure 1. Test set-up.

The test set-up consisted of a driven cylinder head (Figure 1). Only the necessary components needed to drive this exhaust valve were included in the test bench, i.e. a portion of the complete train valve was considered and the forces due to gas ignition were neglected. Pressurized oil was fed into the cylinder head to lubricate the valvetrain by an auxiliary pump. The exhaust valve at cylinder 4 was instrumented with strain gauges at the base of the valve stem, in the zone where fatigue failure is usually found (Figure 2). Signals from the strain gauges were collected using a data acquisition system, with a sampling frequency of 100 kHz.

A special cam profile was used to increase the seating velocity and to magnify the dynamic effect. The cam was designed to generate a closing speed of 2.0 m/s at 3000 r/min (camshaft), which is approximately 10 times the typical closing speed usually found in engines. Figure 3 shows the valvetrain configuration used for the tests. The cam is in contact with the rocker arm and introduces the movement to the mechanism. One end of the rocker is in contact with the valve tip, whereas the other end is in contact with a hydraulic lash adjuster, which keeps the valve clearance at zero. The spring ensures contact between the valve head and the seat during the closing event.

Strain gauges were mounted on the valve stem surface at opposite locations to obtain any bending deformation of the valve, as seen in Figure 2. The strain gauges recorded strain only in the axial direction. Their axial location on the stem was determined with the aim

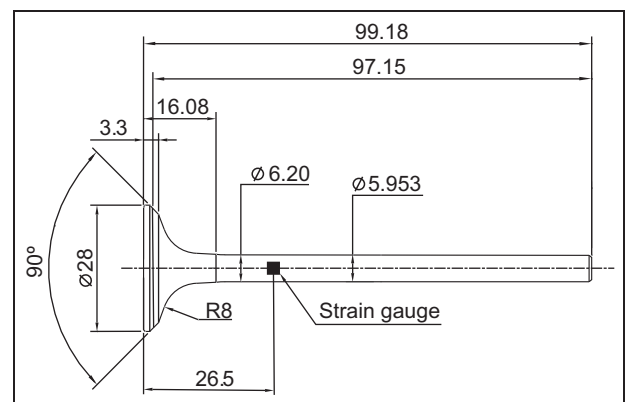


Figure 2. Geometry of the instrumented valve used in the experimental test and in the numerical simulation, and the locations of the strain gauges. The dimensions are given in millimetres.

of obtaining the maximum stresses developed over the part. The valve dimensions used in this work are given in Figure 2.

The tests were performed at room temperature for different camshaft velocities. Figure 4 shows the output of the strain gauges for 1 cycle of valve closure at 640 r/min, which corresponds to a seating velocity of approximately 0.42 m/s. The responses of two diametrically opposed strain gauges are displayed, reflecting both the maximum stresses and the minimum stresses developed at impact.

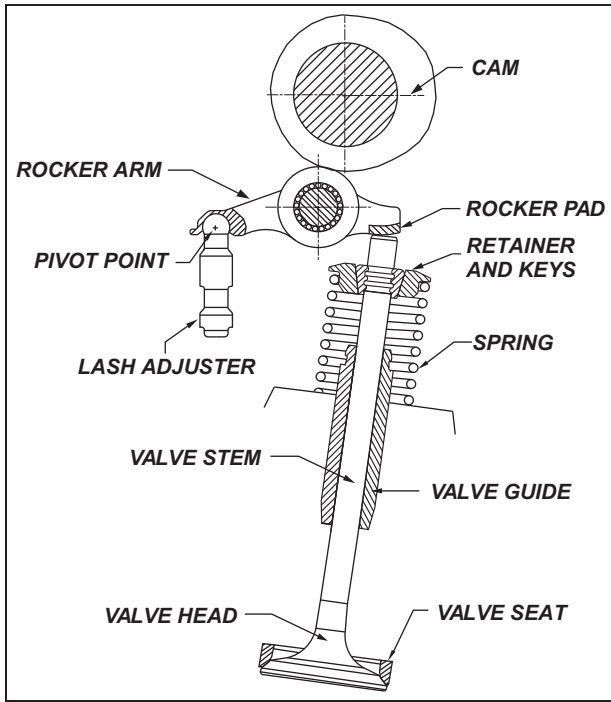


Figure 3. Valvetrain configuration used for the tests.

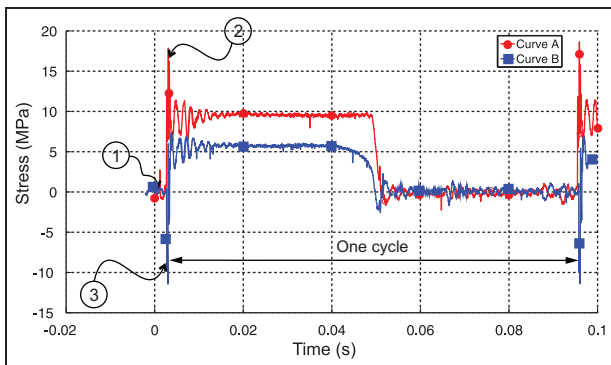


Figure 4. Outputs of the strain gauges for valve closure at 640 r/min.

The details of this effect can be observed in Figure 5, where one strain gauge registers a maximum tensile stress (curve A) and the other indicates a maximum compressive stress (curve B). This is a typical consequence of bending efforts induced by a misalignment between the valve seat and the seat insert. Misalignments can be explained by the following reasons.

1. Frictional forces actuate in the radial direction over the valve tip, induced by the relative motion between the rocker arm and stem.
2. The spring load can be slightly off-centre.
3. The only lateral displacement constraint acting during the valve lift phase is the radial constraint introduced by the valve guide. However, there is a small gap between the valve and the valve guide, allowing for a small misalignment.

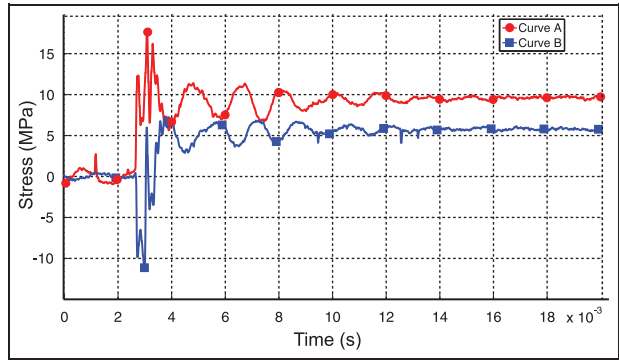


Figure 5. Details of the responses of the strain gauges during impact.

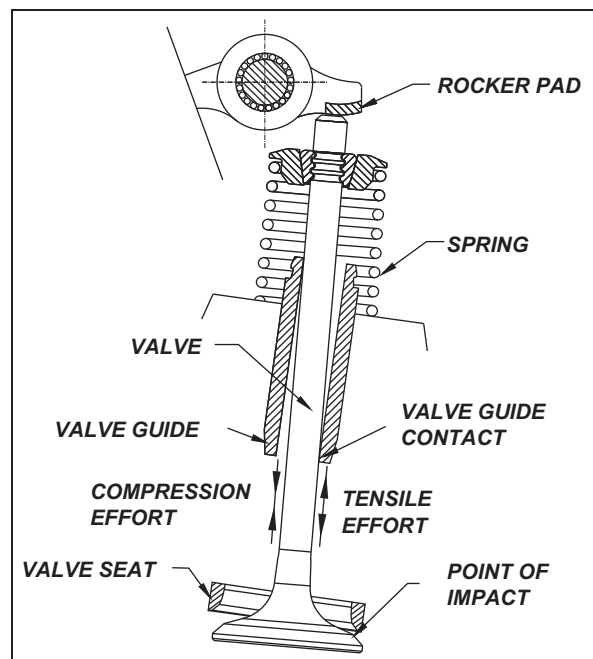


Figure 6. Valve misalignment and related bending efforts during the seating event.

Figure 6 displays a schematic diagram of these potential sources of misalignment. The valve and the seat insert are not concentric during the seating event, and there is a tilt angle between the valve and the valve guide, creating a bending moment. It can be observed that the manufacturing and assembly tolerances play an important role in the valve seating event.

By analysing the experimental output, an initial contact between the valve and the seat insert is identified at point 1 in Figure 4. After this instant, the strain increases until reaching a maximum value (at point 2 on curve A). At the same time, the strain gauge located on the opposite side of the stem registers a compression strain (at point 3 on curve B), indicating a bending deformation of the stem. After this first contact, the stresses on both sides of the valve stem oscillate around zero because of a succession of valve rebounds. Once the valve is in permanent contact with the seat insert,

Table 1. Thermomechanical properties at room temperature of the analysed steel.

Steel	ρ (g/cm ³)	E_{static} (N/mm ²)	Ultimate tensile strength (N/mm ²)
H854	7.7	215×10^3	950–1150

strain waves propagate along the stem. After a while, these oscillations decrease because of damping, and they reach a static value given by the spring preload. The experimental stress curves were calibrated using the spring preload and the area of the valve stem where the strain gauges were located. Therefore, the maximum registered stress is 18 MPa, which is much lower than the yield stress for the test material (1050 MPa; see the valve steel properties in Table 1). This result means that during the impact phase, in the zone of the stem where the strain gauges were situated, the stress state is elastic and no plastic deformations are expected. In fact, a higher stress could be developed in the impact zone; however, the objective of this work is to analyse the maximum stress in the valve stem. The value of 18 MPa is of the same order of magnitude as the classical analytically exact solution of the impact of an elastic bar with a rigid wall, or as the analytical equation reported by Pang et al.¹¹ to calculate the stress in valve stems during the closing event.

As a consequence of the misalignment, the valve impacts the seat at a tilt angle, developing stresses on one side of the stem first. For this reason, the mechanical stress pattern developed during the closing event is 3D, and an axisymmetric FEM model is not able to represent this phenomenon properly. A critical point for the computation of the maximum stresses over the valve stem is the actual eccentricity of the valve with the seat insert due to the manufacturing tolerances, which is identified as the main cause of the valve bending.

The actual values of damping in the system are also of utmost importance to represent the test correctly.

Therefore, the key points for making a correct simulation are to determine the proper values of the following properties:

- the eccentricities of the assembly;
- the damping properties of the materials of both the valve and the insert;
- the numerical damping coefficients at contact;
- the coefficient of friction.

These values were adjusted to match the data registered by the strain gauges during the test.

Definition of the numerical model

Numerical simulations were performed in an attempt to reproduce the experiments as accurately as possible.

The analysis of the stresses and strains in a continuum is made by solving a system of partial differential equations, which state the conditions for equilibrium. Usually, the unknown field in elasticity problems is the displacement $\mathbf{u}(\mathbf{x}, t)$, where \mathbf{x} represents the position vector and t represents the time. In a general form, the elasticity problem consists in finding $\mathbf{u}(\mathbf{x}, t)$ such that

$$\begin{aligned} \operatorname{div}[\boldsymbol{\sigma}(\mathbf{u})] + \mathbf{b} &= \rho \ddot{\mathbf{u}} && \text{in } \Omega \\ \mathbf{u} &= \bar{\mathbf{u}} && \text{on } \Gamma_u \\ \boldsymbol{\sigma} \cdot \mathbf{n} &= \bar{\mathbf{t}} && \text{on } \Gamma_\sigma \end{aligned} \quad (1)$$

where $\boldsymbol{\sigma}$ is the Cauchy stress tensor inside the domain Ω with the outer unit normal \mathbf{n} , ρ is the density, \mathbf{b} is the body force, $\bar{\mathbf{t}}$ is the prescribed traction at the external surface Γ_σ and $\bar{\mathbf{u}}$ is the prescribed displacement at the external surface Γ_u . Dots indicate time differentiation. The discretized weak form of these equations is obtained using the FEM, in which the displacement field is represented as

$$\mathbf{u}(\mathbf{x}, t) = \sum_{i=1}^3 N_i(\mathbf{x}) \mathbf{U}_i(t) \quad (2)$$

where $N_i(\mathbf{x})$ are the finite element shape functions and $\mathbf{U}_i(t)$ are the discrete nodal displacements, which are a function of time t . A detailed explanation has been given in several well-known text-books, e.g. those by Hughes⁹ and Zienkiewicz and Taylor.¹⁰ After replacing equation (2) in the weak form of equation (1), the system of non-linear second-order ordinary differential equations is obtained as

$$\mathbf{M}\ddot{\mathbf{U}}(t) + \mathbf{C}\dot{\mathbf{U}}(t) + \mathbf{K}\mathbf{U}(t) = \mathbf{F}(t) \quad (3)$$

where $\mathbf{F}(t)$ is the loading force vector, $\mathbf{U}(t)$ is the unknown displacements vector and \mathbf{M} , \mathbf{C} and \mathbf{K} are the mass matrix, the damping matrix and the stiffness matrix respectively (they are, in fact, non-linear functions of the displacements $\mathbf{U}(t)$). To solve the non-linear dynamics equation (3), the initial conditions are given as

$$\begin{aligned} \mathbf{U}(0) &= \mathbf{d} \\ \dot{\mathbf{U}}(0) &= \mathbf{v} \end{aligned} \quad (4)$$

where \mathbf{d} and \mathbf{v} are the initial displacement vector and the initial velocity vector respectively.

The equation of motion (3) can be solved using different time-step integration algorithms. In this study, the generalized- α time integration algorithm proposed by Chung and Hulbert²¹ was used. This algorithm can be seen as an evolution of the classical Newmark²² method, in which better control of the dissipation properties is obtained while retaining second-order accuracy for all values of dissipation.

In the generalized- α algorithm, the discrete balance equation

$$\mathbf{M}\mathbf{a}_{n+1-\alpha_m} + \mathbf{C}\mathbf{v}_{n+1-\alpha_f} + \mathbf{K}\mathbf{d}_{n+1-\alpha_f} = \mathbf{F}(t_{n+1-\alpha_f}) \quad (5)$$

is solved at each step, where

$$\begin{aligned}
 \mathbf{d}_{n+1-\alpha_f} &= (1 - \alpha_f)\mathbf{d}_{n+1} + \alpha_f\mathbf{d}_n \\
 \mathbf{v}_{n+1-\alpha_f} &= (1 - \alpha_f)\mathbf{v}_{n+1} + \alpha_f\mathbf{v}_n \\
 \mathbf{a}_{n+1-\alpha_m} &= (1 - \alpha_m)\mathbf{a}_{n+1} + \alpha_m\mathbf{a}_n \\
 t_{n+1-\alpha_f} &= (1 - \alpha_f)t_{n+1} + \alpha_f t_n \\
 \mathbf{d}_{n+1} &= \mathbf{d}_n + \Delta t \mathbf{v}_n + \Delta t^2 \left[\left(\frac{1}{2} - \beta\right)\mathbf{a}_n + \beta\mathbf{a}_{n+1} \right] \\
 \mathbf{v}_{n+1} &= \mathbf{v}_n + \Delta t [(1 - \gamma)\mathbf{a}_n + \gamma\mathbf{a}_{n+1}]
 \end{aligned} \quad (6)$$

with the time stages $n \in \{0, 1, \dots, N\}$, N being the total number of time steps and Δt the time-step increment; the initial values are given by

$$\begin{aligned}
 \mathbf{d}_0 &= \mathbf{d} \\
 \mathbf{v}_0 &= \mathbf{v} \\
 \mathbf{a}_0 &= \mathbf{M}^{-1}[\mathbf{F}(0) - \mathbf{C}\mathbf{v} - \mathbf{K}\mathbf{d}]
 \end{aligned}$$

The generalized- α algorithm can achieve high-frequency dissipation while minimizing unwanted low-frequency dissipation. The algorithm is second-order accurate if the parameters γ , α_m and α_f are linked by the equation

$$\gamma = \frac{1}{2} - \alpha_m + \alpha_f \quad (7)$$

and unconditionally stable if

$$\alpha_m \leq \alpha_f \leq \frac{1}{2}, \beta \geq \frac{1}{4} + \frac{1}{2}(\alpha_f - \alpha_m) \quad (8)$$

A sufficiently small time-step increment was used in the simulations to obtain the high-frequency components excited by the impact, which produced stress waves that propagate along the stem. The spurious high-frequency content was damped out by the algorithm by selecting appropriate values for its parameters. Note also that numerical dissipation was found to be useful to improve the convergence of the iterative equation solver for computing the solution of the contact-impact problem, which is a highly non-linear problem. The addition of the high-frequency dissipation does not produce a loss of accuracy nor introduce excessive algorithmic damping in the important low-frequency modes. Other algorithms, such as the Newmark²² family algorithms,²³ can also provide high-frequency dissipation; however, they are too dissipative in the low-frequency domain and are second-order accurate only in the undamped case.

The spectral radius ρ_∞ of a time integration algorithm is a measure of the dissipation at the highest frequencies. An undamped scheme is characterized by $\rho_\infty = 1$, whereas $\rho_\infty = 0$ provides asymptotic annihilation of the high-frequency response. For the generalized- α method, the parameters α_m and α_f can be defined in terms of the desired value of ρ_∞ as

$$\alpha_m = \frac{2\rho_\infty - 1}{\rho_\infty + 1}, \alpha_f = \frac{\rho_\infty}{\rho_\infty + 1} \quad (9)$$

An optimum relationship between the algorithm parameters was determined by testing, in order to obtain displacement and stress responses free of spurious

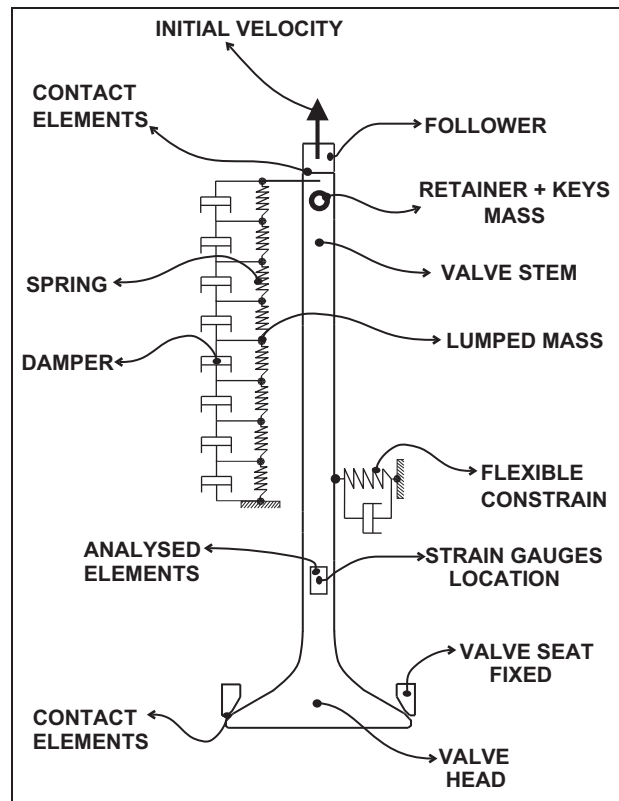


Figure 7. Finite element model.

numerical oscillations and, furthermore, to improve the convergence of the impact problem.

Finite element model

The dynamic simulations were performed using the finite element code SAMCEF.²⁴ A 3D valve model was defined (Figure 7). The valve was modelled using a tetrahedral Delaunay mesh, consisting of 18,465 nodes and 86,748 elements with an average size of 0.65 mm, refined at the contact surfaces. Figure 8 shows the details of the mesh. Based on the experimental results registered by the strain gauges, which indicated no plastic deformations, a linear elastic material model was adopted.

Contact between the valve stem and the valve guide was modelled by non-linear springs. Figure 9 shows the radial stiffness law for these springs. When the displacement is less than 0.02 mm, the spring force is almost zero, representing the valve guide gap. When the spring displacement is greater than this value, the stiffness increases suddenly, simulating contact between the valve and the valve guide.

The return spring was represented by eight spring elements connected in series. Lumped masses were located between the spring elements to consider the distributed mass of the spring, allowing us to obtain the internal dynamics of the spring. Damper elements were included to represent the friction damping generated by the valve stem seal and the valve guide. This friction

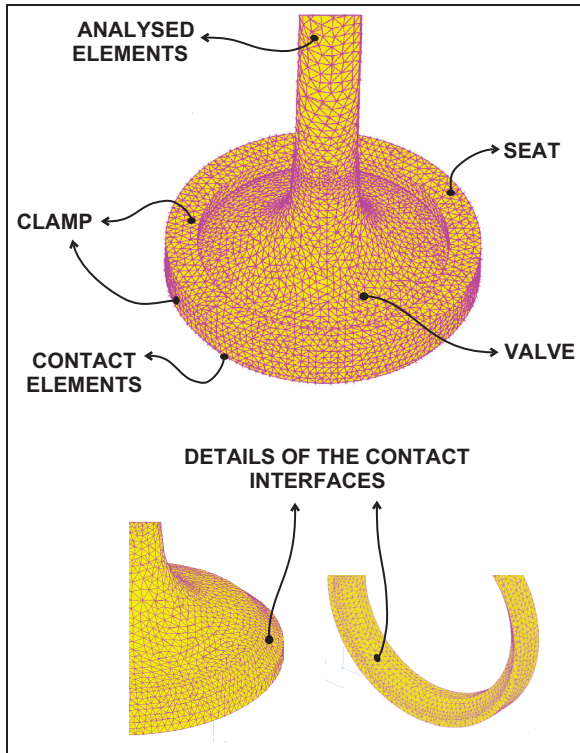


Figure 8. Mesh topology details.

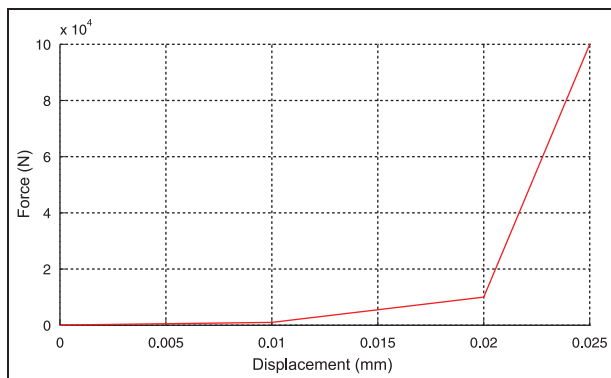


Figure 9. Radial stiffness law for the stem-guide contact.

force provides a resistance to the translation motion of the valve which affects the stress response during the impact event. A lumped mass was situated at the end of the stem, representing the total mass of the retainer and the keys.

The contact between the valve and the seat insert, as well as the contact between the valve tip and the follower, were modelled by a node-to-face contact algorithm based on an augmented Lagrange method proposed by Alart and Curnier²⁵. With this approach, no penetration between the contacting bodies is allowed and, furthermore, the user does not need to tune any parameter, as required by penalty methods, to achieve acceptable solutions.^{26, 27}

The contact is defined between a group of slave nodes and a group of master faces. Friction was considered to simulate the effects that take place because of

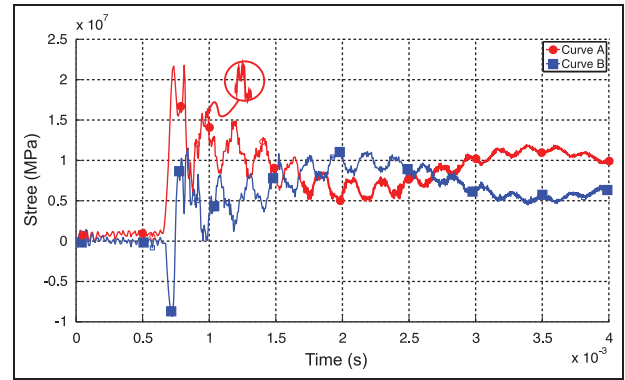


Figure 10. Stress solutions using the generalized- α time integration algorithm with the spectral ratio $\rho_\infty = 1$, for the Newmark scheme.

the relative tangential displacement between the valve and the seat insert.

The following considerations are taken into account when imposing the boundary and initial conditions of the model.

1. Initially, the stem is in contact with the follower.
2. The follower is initially moving with a constant speed equal to the seating velocity.
3. The seat insert is clamped on its top and outside surfaces.
4. The valve and the follower have the same initial velocities.
5. The return spring is preloaded.

Contact elements were defined between the valve and the seat insert and between the valve tip and the follower (Figure 7).

The material is a high-strength austenitic steel alloy (specially developed for valves), with the physical properties at room temperature presented in Table 1. Material damping was included to damp out the stress response at high frequencies.

An automatic time-step control was used, with the minimum time step set to $\Delta t = 10^{-9}$ s, and the maximum time step $\Delta t = 10^{-6}$ s (one tenth of the sampling period of the strain gauges).

The system is initially in equilibrium, loaded by the return spring, and both the valve and the follower are in motion with a constant velocity, which is dependent on both the engine speed and the cam profile. For this particular case, with a camshaft speed of 640 r/min, the valve and follower had an initial velocity of 0.42 m/s.

The response was computed for various values of the algorithm parameters, with the purpose of making a comparison and obtaining a better insight into their influence on the response. An Intel Core i7 processor with a random-access memory of 16 GB of was used in all simulations.

Figure 10 shows the stress curve computed using the spectral ratio $\rho_\infty = 1$ (the value for which the algorithm

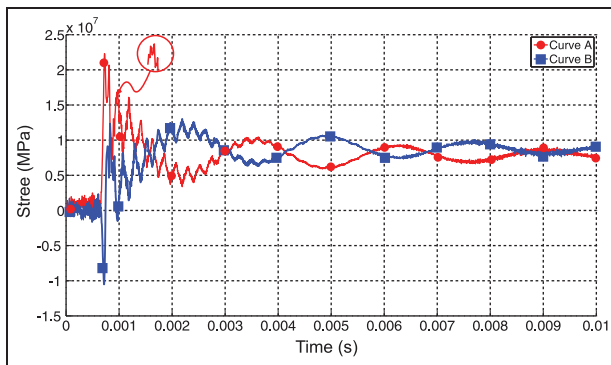


Figure 11. Stress solutions using the generalized- α time integration algorithm with the spectral ratio $\rho_\infty = 0.5$.

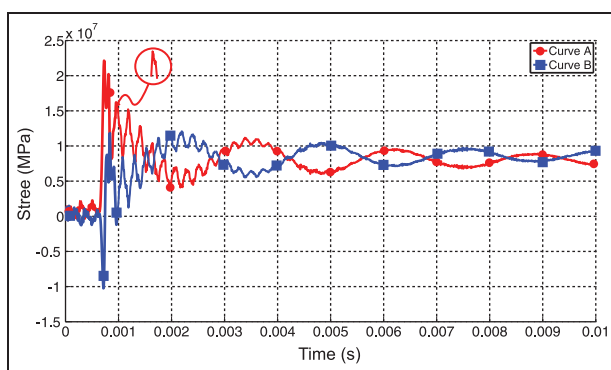


Figure 12. Stress solutions using the generalized- α time integration algorithm with the spectral ratio $\rho_\infty = 0.4$.

coincides with the canonical Newmark scheme, without numerical damping). Figure 10 displays some numerical oscillations attributable to the time integrator. Because of the high frequency of these oscillations, the automatic time-step control sets a very small time step and, therefore, a computer time of 27 h was required for computing a simulation of 0.004 s.

Figure 11 shows the stress curve obtained using the spectral ratio $\rho_\infty = 0.5$. The solution looks quite similar to the $\rho_\infty = 1$ case, and the computation time was also similar.

In Figure 12, the spectral ratio $\rho_\infty = 0.4$ was selected, and a more damped response is obtained. In this case, the computation time was reduced to 11 h because the time-step control was able to select larger time steps. The numerical oscillations were damped out, and a considerable reduction in the computation time was obtained.

Finally, a spectral ratio ρ_∞ equal to zero was proposed, which corresponds to maximum dissipation (Figure 13). In this case, the computation time was reduced to only 3 h.

A value of $\rho_\infty = 0$ was used in the rest of the numerical experiences because the influence on the response was limited to damping out spurious numerical oscillations without affecting the accuracy, and the computation time was a minimum in this case.

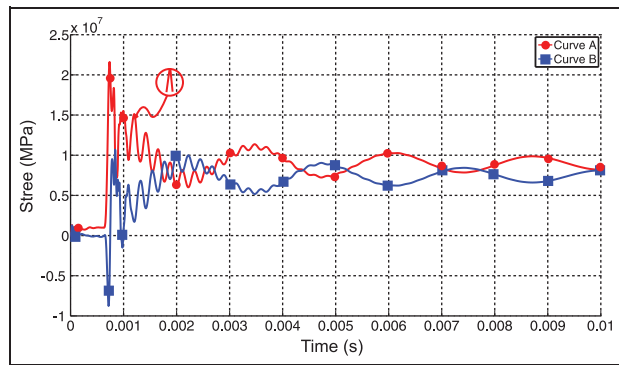


Figure 13. Stress solutions using the generalized- α time integration algorithm with the spectral ratio $\rho_\infty = 0$.

Different configurations of the model were then tested to find the correct values of the misalignment between the guide and the seat and the material damping coefficients.

Both the valve-to-seat insert offset (the eccentricity) and the valve tilt angle were varied until they matched the stress responses observed in the experiments. Finally, a misalignment angle of 0.05° without eccentricity of the valve was found to give the best fit, which is compatible with the manufacturing tolerances of the guide and stem.

The material damping coefficients of both the spring-damper and the valve were adjusted until good agreement between the numerical solution and the experimental results was obtained. After performing several tests, the damping coefficients were identified as follows:

- the damping coefficient of the valve material, 1500 N s/m;
- the damping coefficient of the spring, 500 N s/m;
- the damping coefficient of the valve-to-valve guide, 1000 N s/m.

According to Lewis and Dwyer-Joyce,¹⁹ the coefficient of friction between the valve and the seat ranges from 0.05 for fully lubricated steel on steel, to 0.1 for boundary lubricated steel on steel (this is the usual value for running engine valves) and to 0.4 for completely dry steel on steel. Taking into account that before the tests the valve and the seat were covered by a thin layer of oil (to prevent oxidation), the expected value for the friction coefficient was in the range from 0.15 to 0.3. Different friction coefficients were set in the range from 0.15 to 0.3 in order to understand their effect on the stress response of the valve stem during the closing event. For example, Figure 14 shows the numerical stress curve with $\rho_\infty = 0$ (full numerical damping) and the friction coefficient equal to zero; it can be seen that the curves are not sufficiently damped, particularly for curve B, where the second stress peak at point A is higher than that on the experimental stress curve. The value of the coefficient of

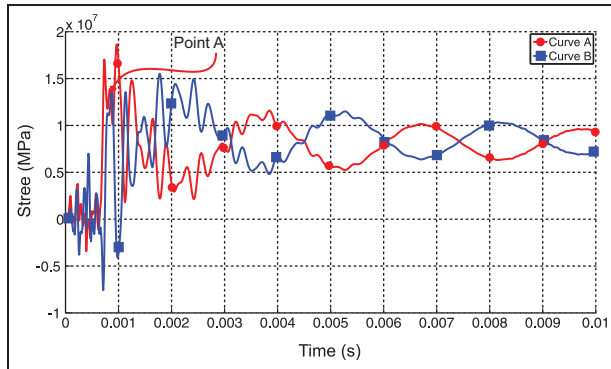


Figure 14. Numerical computation of the stress evolution with the coefficient of friction equal to zero and $\rho_{\infty} = 0$.

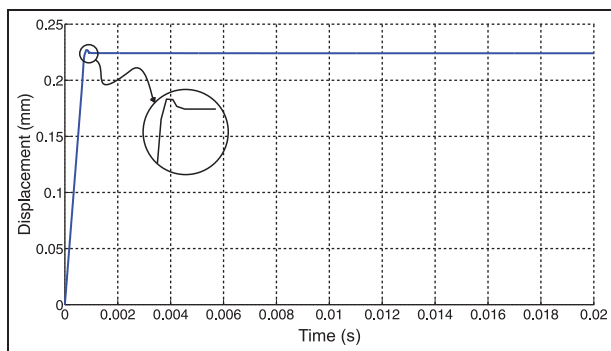


Figure 15. Displacement as a function of time for a node located over the seat surface of the valve.

friction which matched the numerical solution to the empirical results better was 0.2.

Analysis of results

The displacement evolution of a contact node on the valve seat is presented in Figure 15. At the beginning, both the follower and the valve move with the same constant velocity. When the valve makes contact with the seat insert, the motion suddenly stops and the slope of the displacement curve changes.

The misalignment between the valve and the seat insert bends the stem at the initial impact, and opposite sides of the stem reach peak values of 22 MPa (curve A) and -9 MPa (curve B), as shown in Figure 16. These values are compatible with the experimental results, namely 18 MPa for curve A and -11 MPa for curve B, as shown in Figure 4. From Figure 16, it is observed that, after the initial contact–impact time instant, stress oscillations develop which are composed of two main phenomena:

- a high-frequency **tensile stress wave**, with a period of approximately 2×10^{-4} s, which rapidly damps out at time $t \approx 0.0055$ s;
- a low-frequency **bending stress wave**, with a period of approximately 2.5×10^{-4} s, which damps out at time $t \approx 0.02$ s.

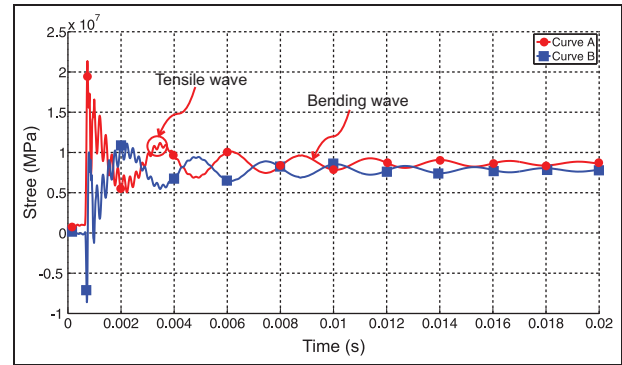


Figure 16. Numerical computation of the stress evolution.

The amplitudes of both stress waves decrease in time, and the stresses on the opposite sides of the stem converge to stationary values of nearly 6 MPa and 10 MPa, which coincide with the experimental observations. These values are consistent with the remaining static bending induced by the return spring load.

The peak value of stress that appears on the valve stem after impact with the seat insert is of utmost importance for design verification by the fatigue criteria.

Note that the stress results that were obtained with the proposed finite element model are in good agreement with the experimental data, validating the finite element model. This numerical model permits us to explain clearly the complex phenomena observed in the experimental measurements and will be suitable for design purposes.

Conclusions

A detailed numerical model of the closing event of an internal-combustion engine valve was developed, and the model was validated by comparison with experimental stress measurements. As a result, a better understanding of the valve closing event mechanism was found, showing the important role played by the misalignment between the valve and the seat.

A 3D finite element model, which was able to predict the evolution of the mechanical stresses with time on the valve during the closing event, was presented. Important aspects of this model are as follows.

- High-frequency dissipation was introduced by using the generalized- α time integration algorithm, minimizing low-frequency dissipation and eliminating spurious high-frequency oscillations.
- A very short time step was required to be able to obtain all the harmonics and maximum peak stresses.

The model allowed an analysis with a complete configuration and with a very fine discretization in a reasonable computer time. It is important to remark that

these capabilities of the generalized- α method are essential in industry, which needs to verify or to propose new designs in reasonable times.

The stresses computed with the finite element analysis were in good agreement with the experimental data. Therefore, the proposed model can be used with confidence for verification of new valve designs against pre-defined fatigue criteria.

Valve misalignment cannot be avoided because it is a consequence of the manufacturing and assembly tolerances of the valvetrain components. A conclusion of the study is that, to minimize the sensitivity to fatigue failure, the design should take into account factors leading to increased misalignment, such as the frictional force between the valve tip and the follower, and the misalignment of the elastic force generated by the return spring which actuates on the valve stem end. These forces have to be minimized to avoid increases in the factors that could lead to possible fatigue damage.

Future work will address an extension of the contact algorithm used in this work,^{28–30} with the objectives of obtaining predictions of the contact pressure and using these pressure predictions for prediction of the wear effects between the valve and the seat and between the cam and cam-tappet components. To validate the numerical solutions, a wear-testing machine for motor valves was designed and constructed which reproduces conditions similar to those existing in a combustion engine. A similar machine has been described in the paper by Chun et al.³¹

Acknowledgements

The authors gratefully acknowledge the help and contribution of several colleagues, including Rômulo PF de Almeida, Everton G Leopoldo, Jefferson L de Andrade, Rodolfo Díaz Terrado, Oreste Berta and the Oreste Berta SA team.

Funding

This work was supported by the Consejo Nacional de Investigaciones Científicas y Técnicas (PIP 2473), Agencia Nacional de Promoción Científica y Tecnológica (PID 398) and Universidad Nacional del Litoral (CAI+D2009 PI65-330 CAI + D 2009 PI65-330).

Declaration of conflicting interest

The authors declare that there is no conflict of interest.

References

1. Cavalieri FJ. *Multiaxial fatigue and wear design in mechanical components at high temperature* (in Spanish). Doctoral Thesis, Universidad Nacional del Litoral, Argentina, 2010, [http:// bibliotecavirtual.unl.edu.ar:8180/tesis/handle/1/200](http://bibliotecavirtual.unl.edu.ar:8180/tesis/handle/1/200) (2010, accessed 4 April 2013).
2. Wagner D, Cavalieri F, Bathias C and Ranc N. Ultrasonic fatigue tests at high temperature on an austenitic steel. *Propulsion Power Research* 2012;1(1): 29–35.
3. Jones DR. Fatigue behavior of exhaust valve alloys. SAE paper 800315, 1980.
4. Teodorescu M, Kushwaha M, Rahnejat H and Taraza D. Elastodynamic transient analysis of a four-cylinder valve train system with camshaft flexibility. *Proc IMechE Part K: J Multi-body Dynamics* 2005; 219(1): 13–25.
5. Teodorescu M, Votsios V, Rahnejat H and Taraza D. Jounce and impact in cam-tappet conjunction induced by the elastodynamics of valve train system. *Meccanica* 2006; 41(2): 157–171.
6. Rahnejat H. *Multi-body dynamics: vehicles, machines and mechanisms*. London: Professional Engineering Publishing Limited, 1998.
7. Roth G. Fatigue analysis methodology for predicting engine valve life. SAE paper 2003-01-0726, 2003.
8. Roth G. Simulation of an engine valve stress/strain response during a closing event. SAE paper 2003-01-0727, 2003.
9. Hughes TJR. *The finite element method. linear and dynamic finite element analysis*. New York: Dover Publications, 2000.
10. Zienkiewicz OC and Taylor RL. *The finite element method, Vol 1: The basis*. 5th edition. Oxford: Butterworth–Heinemann, 2000.
11. Pang ML, Smith SP, Herman R and Buck B. Stress analysis of an automotive engine valve by finite element methods. SAE paper 2006-01-0017, 2006.
12. Rivola A, Troncossi M, Dalpiaz G and Carlini A. Elastodynamic analysis of the desmodromic valve train of a racing motorbike engine by means of combined lumped/finite element model. *Mech System Signal Processing* 2007; 21: 735–760.
13. Teodorescu M, Votsios V and Rahnejat H. Multiphysics analysis for the determination of valvetrain characteristics. *Proc IMechE Part D: J Automobile Engineering* 2005; 219(9): 1109–1117.
14. Kushwaha M, Rahnejat H and Jin ZM. Valve-train dynamics: a simplified tribo-elasto-multi-body analysis. *Proc IMechE Part K: J Multi-body Dynamics* 2000; 214(2): 95–110.
15. Votsios V. *Contact mechanics and impact dynamics of non-conforming elastic and viscoelastic semi-infinite or thin bonded layered solids*. PhD Thesis, Loughborough University, Loughborough, UK, 2003.
16. Konvopoulos K and Gong ZQ. Effect of surface patterning on contact deformation of elastic–plastic layered media. *Trans ASME, J Tribol* 2003; 125: 16–24.
17. Ovaert T and Pan J. Optimal design of layered structures under normal (frictionless) contact loading. *Trans ASME, J Tribol* 2002; 124: 438–442.
18. Teodorescu M and Rahnejat H. Mathematical modelling of layered contact mechanics of cam–tappet conjunction. *Appl Mathl Modelling* 2007; 31: 2610–2627.
19. Lewis R and Dwyer-Joyce RS. *Automotive engine valve recession*. London: Professional Engineering Publishing Limited, 2002.
20. Oreste Berta SA. Home, <http://www.oresteberta.com> (2013, accessed 4 April 2013).
21. Chung J and Hulbert G. Time integration algorithm for structural dynamics with improved numerical dissipation:

- the generalized- α method. *Trans ASME, J ApplMech* 1993; 60(2): 371–375.
22. Newmark NM. A method of computation for structural dynamics. *J Engng Mech Div ASCE* 1959; 85(EM3): 67–94.
 23. Rahnejat H. Computational modeling of problems in contact dynamics. *Engng Analysis* 1985; 2(4): 192–197.
 24. LMS. LMS Samtech, <http://www.lmsintl.com/simulation/samtech/> (2012, accessed 4 April 2013).
 25. Alart P and Curnier A. A mixed formulation for frictional contact problems prone to Newton like solution methods. *Comput Meth Appl Mech Engng* 1991; 92: 353–375.
 26. Cavalieri FJ and Cardona A. An augmented Lagrangian method to solve three-dimensional nonlinear contact problems. *Latin American Appl Research* 2012; 42(201): 281–89.
 27. Cavalieri FJ and Cardona A. An augmented Lagrangian technique combined with a mortar algorithm for modeling mechanical contact problems. *Int J Numer Meth Engng* 2013; 93: 420–442.
 28. Virlez G, Cardona A, Bruls O and Duysinx P. Modelling of frictional unilateral contact in automotive differentials. In: *5th International conference on advanced computational methods in engineering*, Liège, Belgium, 14–17 November 2011.
 29. Fessler H and Ham R. Lubrication and stress analysis as a basis for camshaft optimization. In: *18th FISITA congress, the promise of new technology in the automotive industry*, Torino, Italy, 7–11 May 1990, paper 3957. Warrendale, Pennsylvania: SAE International.
 30. Teodorescu M, Taraza D, Henein N and Bryzik W. Simplified elastohydrodynamic friction model of the cam-tappet contact. SAE paper 2003-01-0985, 2003.
 31. Chun K, Hong J, Lee H, Kim D and Kiu IMJ. A study on engine valve and seat insert wearing depending on speed change. SAE paper 2004-01-1655, 2004.

Appendix I

Notation

\mathbf{b}	body force
\mathbf{C}	damping matrix
\mathbf{d}_0	initial displacement vector
$\mathbf{F}(t)$	loading force vector
\mathbf{K}	stiffness matrix
\mathbf{M}	mass matrix
$N_i(\mathbf{x})$	shape functions
t	time
$\bar{\mathbf{t}}$	prescribed traction
$\mathbf{u}(\mathbf{x}, t)$	displacement vector
$\bar{\mathbf{u}}$	prescribed displacement
$\mathbf{U}_i(t)$	discrete nodal displacements
\mathbf{v}_0	initial velocity vector
\mathbf{x}	position vector
$\alpha_f, \alpha_m, \beta$	coefficients for the generalized- α time integration algorithm
ρ	density
ρ_∞	spectral ratio for the generalized- α time integration algorithm
$\boldsymbol{\sigma}$	Cauchy stress tensor

Abbreviation

FEM	finite element method
-----	-----------------------